Laboratory measurements of vortex-induced sediment pickup rates

Cheng, Nian-Sheng; Emadzadeh, Adel

2016

Cheng, N.-S., & Emadzadeh, A. (2016). Laboratory measurements of vortex-induced sediment pickup rates. International Journal of Sediment Research, in press.

https://hdl.handle.net/10356/80294

https://doi.org/10.1016/j.ijsrc.2016.04.005

Laboratory measurements of vortex-induced sediment pickup rates

Nian-Sheng Cheng[1] and Adel Emadzadeh[2]

[1]School of Civil and Environmental Engineering, Nanyang Technological University Nanyang Avenue, Singapore, 639798. Email: cnscheng@ntu.edu.sg

[2]School of Civil and Environmental Engineering, Nanyang Technological University Nanyang Avenue, Singapore, 639798. Email: aemadzadeh@ntu.edu.sg

Abstract

In the present study, vortices were generated in open channel flow with a cross-flow cylinder installed horizontally near the bed. Sediment pickup rates were then measured over the channel bed downstream the cylinder using a sediment lift. The experimental data show that the pickup rate increases exponentially in the presence of vortices. Two different relationships can be clearly observed between the pickup rate and the maximum root-mean-square (rms) value of the streamwise velocity fluctuation, one for the cylinder-obstructed flow and the other for the unobstructed flow. The results imply that the vortex-induced sediment pickup cannot be explained based on the traditional boundary layer theory.

Introduction

Vortices form when flow passes around a bluff structure. They can move with the flow, distorting by themselves and interacting with each other. Vortices have been a subject of interest to engineers and scientists for decades, but they are complex and an understanding of their mechanism still remains a challenging task. For example, vortices in a cylinder wake may involve interactions with a boundary layer, a separating free shear layer and a wake (Williamson, 1996). A moving vortex carries itself some momentum and energy. When approaching a sediment bed, a vortex could modify significantly near-bed flow properties and thus sediment pickup rates.

Cheng et al.'s (2003) measurements show that downstream a cross-flow cylinder, the fluctuation in the bed shear stress increases significantly, up to 102% of the mean bed shear stress, which appears closely associated with the vortex shedding. Sumer et al. (2003) observed that in the wake of a cross-flow cylinder, the local bedload transport rate could be 50 times higher than that induced by the same mean bed shear stress in a uniform open channel flow. Hopfinger et al. (2004) presented experimental results on sediment erosion by a plane wall jet, showing that sediment transport is primarily affected by streamwise vortices that create sediment streaks or ridges.

In the present study, sediment pickup experiments were conducted in open channel flows obstructed by a cross-flow cylinder, which was installed horizontally near the channel bed. The simple experimental setup, similar to that reported by Cheng et al. (2003), was able to generate vortices that enhance near-bed turbulence and thus sediment entrainment. Both flow velocity and sediment pickup rate were measured at several sections downstream the cylinder for the obstructed flow and also for the unobstructed flow (without any installation of cylinder). The results show that in the presence of vortex, the local pickup rate increases

with increasing turbulence intensity, but following a trend different from that for the unobstructed flow.

Experimental setup

Experiments were conducted in a tilting flume (14 m long, 0.6 m wide and 0.6 m deep) with glass walls and a steel bed. The flume was equipped with a sediment lift, similar to that used by van Rijn (1984), which was attached to the channel bottom through a rectangular opening, 1.5 cm in the streamwise direction and 10 cm in the lateral direction, and installed at the section 9 m from the flume entrance (Fig. 1). Sediment particles were lifted up at a constant rate through the bed opening with a piston driven by an electrical motor. The piston speed and therefore the sediment supply rate can be adjusted by a control box. In addition, using a gear box, the piston speed could be reduced to 0.2 mm/min to facilitate low pickup rate measurements.

The volumetric pickup rate E was measured as $V_T(1-\varepsilon)/(AT)$, where A is the area of the bed opening, T is the time duration for pickup measurement, and V_T is the bulk volume of the entrained sediment calculated as the product of A and the piston displacement measured by the dial gauge, and ε is the average bed porosity. Three uniform sediments of median diameter D = 0.23, 0.44 and 0.86 mm were used, and the measured average porosity was 0.44, 0.43 and 0.40, respectively. The density of sediment grains ρ_s = 2650 kg/m^3. The critical shear velocity for the incipient sediment motion, which was calculated with the Shields diagram or Whitehouse et al.'s (2000) empirical formula, is equal to 0.013, 0.015 and 0.021 m/s, respectively. It should be mentioned that for each size of sediment tested, a layer of the same sediment particles was also glued onto the channel bed to ensure a consistent roughness throughout the channel.

Prior to each experiment, the flume was filled with water to a certain level and then the sediment lift was loaded with sediment particles to be tested. After the channel flow stabilized as desired, the piston speed was adjusted slowly so that only a single layer of moving particles was observed over and downstream the bed opening. At this stage, the piston displacement and the corresponding time duration were recorded.

During preliminary experiments, it was observed that there would be a pit over the observation area if sediment injection rate was smaller than the entrainment and a hump if injection rate was higher than the entrainment. The existence of a hump/hip would definitely affect the local flow field and thus the sediment entrainment. To minimize such uncertainties, the sampling time was taken long enough to cover several sequences of hump and pit occurrence. This resulted in an average measurement of the pickup rate for each particular test. In addition, to enhance the quality of the pickup measurement, the observation for each individual test was repeated at least five times to ensure that there was less than 15 % difference among different measurements of pickup rates.

The observed pickup rate varied from 4.6×10^{-7} to 4.0×10^{-4} m/s. If the bed porosity is taken to be 0.42, the rate of change in the bed level can be calculated to be in the range of 1.1×10^{-6} to 9.5×10^{-4} m/s. In comparison, the measured near-bed flow velocity was more than 0.3 m/s. Therefore, the near-bed flow velocity was at least 300 times higher than the rate of change of the bed level. In addition, it is noted that the rms value of the velocity fluctuation in the streamwise direction varied from 0.034 to 0.175 m/s, which was at least 35 times higher than the rate of change of the bed level. Given the large differences, the effect of the change in the bed level on the near-bed flow field could be considered negligible.

To generate vortices, a horizontal cylinder (diameter = 2.6 cm) was installed across the channel upstream the sediment lift, with a gap of 2 cm above the bed (Fig. 1). The gap chosen was found not to suppress the vortex shedding or to change its frequency (Sumer &

Fredsøe, 2006). Different levels of turbulence were achieved at the test section by varying the distance from the cylinder location to the test section. By trial and error through a preliminary test, it was found that when the distance varied from x = 10 cm to 30 cm (see Fig. 1), considerable variations were observed in the flow turbulence but relatively small in the mean flow velocity.

All measurements were carried out by setting the flow depth H at 20 cm and the bed slope at 0.0005. Four different flow rates were applied for each size of sediment. For each series of experiments with a fixed flow rate, flow velocity and pickup rate were measured under both obstructed and unobstructed flow conditions. For the obstructed flows, with the cylinder installed upstream the test section, five tests were completed with five different x-values (i.e. x = 10, 15, 20, 25 and 30 cm). An additional test with the same flow rate was also conducted for the unobstructed flow, i.e. without any installation of cylinder. This may represent an equivalent case with a large x-value, for which the cylinder appears far away from the test section so that the vortex effect is negligible.

Flow velocity measurements were carried out using a three-component down-looking Acoustic Doppler Velocimeter (ADV). The ADV was positioned at the flume centerline right above the sediment lift and velocity measurements were completed prior to or after the pickup measurements. When conducting flow velocity measurements at the test section, the bed opening where the sediment lift was installed was covered, and its surface level was flush with the surrounding fixed bed. Therefore, the mobile bed over the bed opening had no effect on the flow measurements. For each velocity profile, 23-25 points were sampled at a rate of 50 Hz for three minutes. The shear velocity u_* for the unobstructed flow was estimated by fitting the logarithmic law to the velocity profile measured in the near-bed zone about 25% of

the flow depth. Further information related to the experimental setup is given in Emadzadeh (2014).

Results

In total 72 experiments were completed and the data are summarised in Table 1. Fig. 2 shows an example of the profiles of the streamwise mean flow velocity u for the cross-sectional average velocity U = 0.59 m/s and the sediment median diameter D = 0.23 mm. Though being different from the velocity profile for the unobstructed flow, the five velocity profiles downstream the cylinder are very close to each other. The small difference in the cylinder-affected velocity profiles can be explained by the relatively small cylinder size compared to the flow depth and also the small streamwise reach (x = 10 - 30 cm) which covered the selected cylinder locations.

Figs. 3 to 5 shows the profiles of u_{rms}, v_{rms} and w_{rms}, which denote the root-mean-square (rms) values of the velocity fluctuation in the streamwise, lateral and vertical direction, respectively, for U = 0.59 m/s and D = 0.23 mm. Being different from the small variations among the mean velocity profiles, the level of turbulence downstream the cylinder varied significantly. For example, the maximum value of u_{rms} increased from 5.9 cm/s for the unobstructed flow to 10.5 cm/s (about 1.8 times higher) for the obstructed flow with the cylinder at x = 30 cm, and 17.2 cm/s (about 2.9 times higher) with the cylinder at x = 10 cm. Similar variations can be observed in the maximum values of v_{rms} and w_{rms}. Fig. 6 plots the profiles of the relative turbulence intensity u_{rms}/u for U = 0.59 m/s and D = 0.23 mm. It can be seen that the maximum value of u_{rms}/u increases from 13% for the unobstructed flow up to 45% for the obstructed flow.

Fig. 7 show the variation of the pickup rate E with the maximum value of u_{rms} for U = 0.59 m/s and D = 0.23 mm, which was measured with the cylinder installed at the five different distances from the test section. When the cylinder was situated about 25-30 cm upstream the test section, the pickup rate measured at the test section is still comparable to that measured under the unobstructed flow condition. However, when the cylinder approaches the test section (i.e. x = 10-20 cm), the pickup rate increases exponentially with increasing maximum value of u_{rms}.

In Fig. 8, four series of data collected for four different flow rates are plotted together for the case of D = 0.23 mm to show the variation of E with the maximum values of u_{rms}. It can be seen that in spite of the four flow rates applied, E measured downstream the cylinder varies in a way that is clearly different from that measured under the unobstructed flow condition. This implies that a different mechanism exists for sediment entrainment in the presence of vortex, which will be discussed subsequently. For the obstructed flows, the data points are plotted using the filled symbols. The four series of data seem to follow a single trend line. In comparison, another trend line also exists, being represented by the four data points (plotted with the open symbols) measured for the unobstructed flows.

Fig. 9 is similar to Fig. 8, but including all the data collected for various flow and bed configurations with the three sizes of sediments. It seems that the data points group according to the sediment size in some way, but the difference is not large. However, as a whole, all the data measured for the obstructed flows vary following a different trend from those for the unobstructed flows.

The results suggest that the sediment pickup enhanced by vortices may not be explained based on the traditional boundary layer theory, which applies only for the unobstructed open channel flow. In open channel flow without any obstruction, the

turbulence intensity near the bed (which can be represented by the maximum value of u_{rms}) varies in a limited range, and it can be quantified using the shear velocity u_* (Nezu & Nakagawa, 1993). Therefore, E can be expressed as a function of u_* and D for given fluid and sediment properties (Van Rijn, 1984). In the presence of vortices, u_* is difficult to measure and thus not a suitable variable for the description of E. However, it can be reasonably replaced with the maximum value of u_{rms}, as demonstrated in the present study.

In the following, E, $u_{rms,max}$ and D are first normalized as

$$E_* = \frac{E}{\sqrt{\Delta g D}} \tag{1}$$

$$u^*_{rms,\max} = \frac{u_{rms,\max}}{\sqrt{\Delta g D}} \tag{2}$$

$$D_* = \left(\frac{\Delta g}{\nu^2}\right)^{1/3} D \tag{3}$$

where Δ [= $(\rho_s - \rho)/\rho$] is the effective specific density with ρ_s and ρ denoting the grain and fluid density, respectively, g is the gravitational acceleration, D is the grain diameter and ν is the kinematic viscosity of fluid (which was taken to be 8.6×10^{-7} m^2/s in the present study). Then it is assumed that the dimensionless pickup rate E_* can be expressed as a function of D_* and $u^*_{rms,\max}$ in the power form,

$$E_* = aD_*^b (u^*_{rms,\max})^c \tag{4}$$

where a, b and c are constants. It should be mentioned that the functional form in Eq. (4) is purely empirical. However, similar functions have also been employed in previous studies by Van Rijn (1984) and Cao (1997). Based on his own data, Van Rijn (1984) proposed that the dimensionless pickup rate is related to D_* and a transport-stage parameter related to the Shields number. Cao (1997) attempted to theoretically derive a pickup function by associating sediment entrainment with turbulence bursts. Both studies have demonstrated that

a function in the power form can be used to reasonably describe the dependence of the pickup rate on the dimensionless grain diameter and Shields number.

To quantify the goodness of fit of the proposed power function, the Pearson product-moment correlation coefficients (i.e. Pearson's R) were calculated. Fig. 9 presents the variation of R^2 with b, where R is the correlation coefficient of $\log(E_*/D_*^b)$ and $\log(u^*_{rms,\max})$. It can be seen that R^2 achieves its maximum 0.91 at $b \approx 2.5$. Fig. 10 shows the relation of $E_*/D_*^{2.5}$ against $u^*_{rms,\max}$, which can be described using the following function,

$$E_* = 0.00015 D_*^{2.5} u^*_{rms,\max} \exp(-\frac{6.2}{u^*_{rms,\max}}) \quad (5)$$

It should be mentioned that Eq. (5) is empirical and the data used vary in the limited range (e.g. D = 0.23-0.86 mm).

Discussions

In the above data analysis, we only involve the velocity fluctuation in the streamwise direction, $u_{rms,max}$. For comparison, the analysis can be further extended by considering the velocity fluctuation in the lateral direction, $v_{rms,max}$, and also that in the vertical direction, $w_{rms,max}$. This yields two more empirical formulas, one based on $v_{rms,max}$,

$$E_* = 0.00045 D_*^{2.1} v^*_{rms,\max} \exp(-\frac{5.7}{v^*_{rms,\max}}) \quad (6)$$

and the other based on $w_{rms,max}$,

$$E_* = 0.0001 D_*^{2} w^*_{rms,\max} \exp(-\frac{3.5}{w^*_{rms,\max}}) \quad (7)$$

where $v^*_{rms,\max} = v_{rms,\max} / \sqrt{\Delta g D}$ and $w^*_{rms,\max} = w_{rms,\max} / \sqrt{\Delta g D}$. Eqs. (6) and (7) are plotted in in Figs. 12 and 13, respectively, together with the experimental data. From the figures, it can be observed that (1) the correlation obtained based on $u_{rms,max}$ (streamwise component) is similar to that based on $v_{rms,max}$ (lateral component), and (2) the correlations based on $w_{rms,max}$ (vertical component) is worse than that based on $u_{rms,max}$ or $v_{rms,max}$. This result indicates that the pickup rate could be more closely related to the velocity fluctuations in the streamwise and lateral direction than that in the vertical direction. This is to some extent against expectations, and thus further research is needed to explore the difference.

The experimental data collected in the present study show two different trends of variations in the sediment pickup rate. When the horizontal cylinder approaches the test section, the near-bed turbulence is affected dominantly by the cylinder-generated vortex. The enhanced turbulence results in significant increases in the sediment pickup rate. If the cylinder is moved step by step towards upstream, the vortex effect will gradually lessen. Eventually, when the distance from the cylinder to the test section becomes relatively large, the vortex effect can be considered negligible and then the near-bed turbulence is finally dominated by the boundary shear. In the above data analysis, we only use the rms value of velocity fluctuations to quantify the level of turbulence that was generated by the boundary shear, vortex or both. However, due to the different mechanisms, the turbulence generated, even with the same value of u_{rms}, may have different effects on the sediment pickup rate. This is evident in Fig. 8. It can be seen that at the same value of u_{rms}, the pickup rate could become more than ten times higher for the turbulent flow dominated by boundary shear, in spite of the fact that both U and D remain unchanged. This suggests that in a unidirectional flow, vortex-induced turbulence may not be efficient in sediment entrainment in comparison to turbulent flow dominated by boundary shear.

In this study, the vortex was generated by the horizontal cross-flow cylinder. However, in river flows, near-bed vortex and turbulence can be associated with difference mechanisms of generation, which is much more complicated, for example, in bedform and channel migration (Simons et al., 1965; Sun et al., 2015) and unsteady sediment transport (Wang et al., 2015). The result presented in this paper may not be applicable for other cases with enhanced near-bed turbulence, but similar correlations could still exist between the pickup rate and the maximum rms velocity.

Summary

Both flow velocity and sediment pickup rate were measured at the same flow depth for unobstructed and obstructed open channel flows. The obstructed flow involved vortices generated by a cross-flow cylinder near the bed. By varying the distance between the test section and the cylinder upstream, different levels of turbulence occurred and therefore the pickup rate varied at the test section. The measurements show that the pickup rate increases exponentially in the presence of vortices, and it correlates well with the maximum rms value of the streamwise or lateral flow velocity fluctuation. However, two separate variations of the pickup rate with the level of turbulence can be observed for the unobstructed and obstructed flow conditions. Future efforts are needed to generally quantify effects of the turbulence induced by boundary shear and/or vortices on the sediment pickup rates.

References

Cao, Z. X. (1997). Turbulent bursting-based sediment entrainment function. *Journal of Hydraulic Engineering-Asce, 123*(3), 233-236. doi:10.1061/(asce)0733-9429(1997)123:3(233)

Cheng, N. S., Sumer, B. M., & Fredsoe, J. (2003). Investigation of bed shear stresses subject to external turbulence. *International Journal of Heat and Fluid Flow, 24*(6), 816-824. doi:10.1016/s0142-727x(03)00088-2

Emadzadeh, A. (2014). *Experimental investigation of turbulence effects on sediment pickup rate in open channel flows.* (Ph.D Thesis), Nanyang Technological University, Singapore.

Hopfinger, E. J., Kurniawan, A., H., G. W., & U., l. (2004). Sediment erosion by Görtler vortices: the scour-hole problem. *Journal of Fluid Mechanics, 520*, 327-342. doi:10.1017/S0022112004001636

Nezu, I., & Nakagawa, H. (1993). *Turbulence in Open-Channel Flows*. Rotterdam, Netherland: A.A. Balkema.

Simons, D. B., Richardson, E. V., & Nordin, C. F. J. (1965). *Bedload equation for ripples and dunes* (Geological Survey Professional Paper 462-H). Retrieved from United States Government Printing Office, Washington:

Sumer, B. M., Chua, L. H. C., Cheng, N. S., & Fredsoe, J. (2003). Influence of turbulence on bed load sediment transport. *Journal of Hydraulic Engineering-Asce, 129*(8), 585-596. doi:10.1061/(asce)0733-9429(2003)129:8(585)

Sumer, B. M., & Fredsøe, J. (2006). *Hydrodynamics around cylindrical strucures*. Singapore: World Scientific Publishing Co Pte Ltd.

Sun, J., Lin, B. L., & Kuang, H. W. (2015). Numerical modelling of channel migration with application to laboratory rivers. *International Journal of Sediment Research, 30*(1), 13-27.

Van Rijn, L. C. (1984). Sediment pick-up functions. *Journal of Hydraulic Engineering-Asce, 110*(10), 1494-1502.

Wang, L., Cuthbertson, A. J., Pender, G., & Cao, Z. (2015). Experimental investigations of graded sediment transport under unsteady flow hydrographs. *International Journal of Sediment Research, 30*(4), 306-320.

Whitehouse, R. J. S., Soulsby, R. L., & Damgaard, J. S. (2000). Inception of sediment transport on steep slopes - Discussion. *Journal of Hydraulic Engineering-Asce, 126*(7), 553-555.

Williamson, C. H. K. (1996). Vortex dynamics in the cylinder wake. *Annual Review of Fluid Mechanics, 28*, 477-539. doi:10.1146/annurev.fl.28.010196.002401

(a)

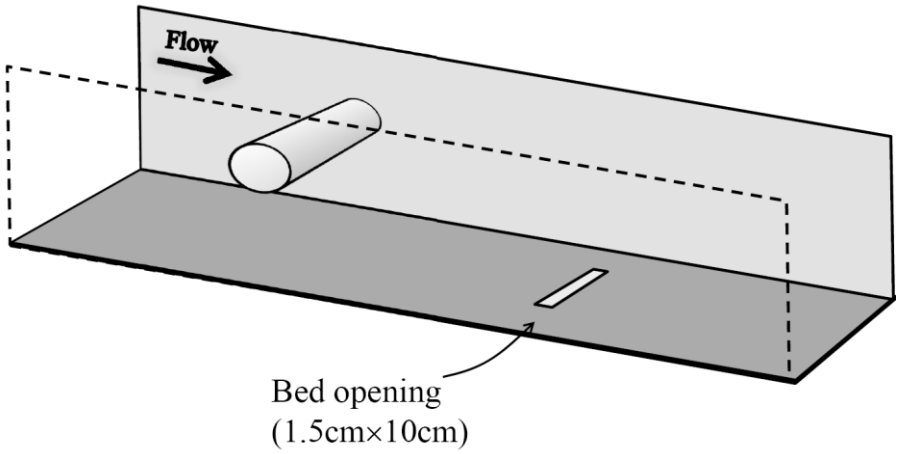

(b)

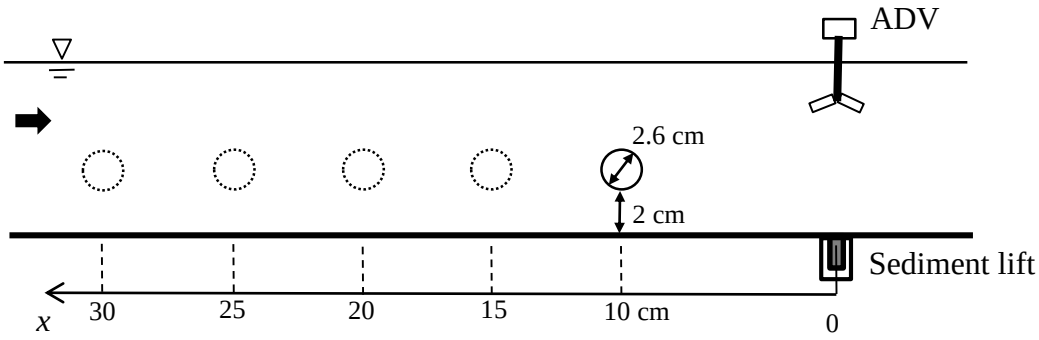

Fig. 1. Experimental setup: (a) 3D sketch; and (b) side view (not to scale).

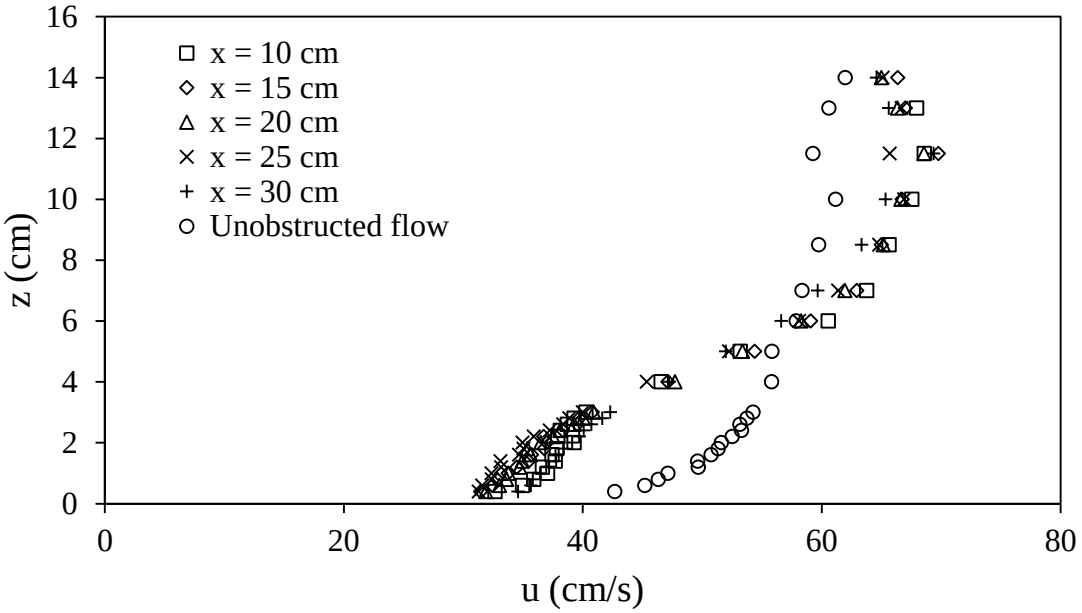

Fig. 2. Profiles of streamwise mean flow velocity for U = 0.59 m/s and D = 0.23 mm

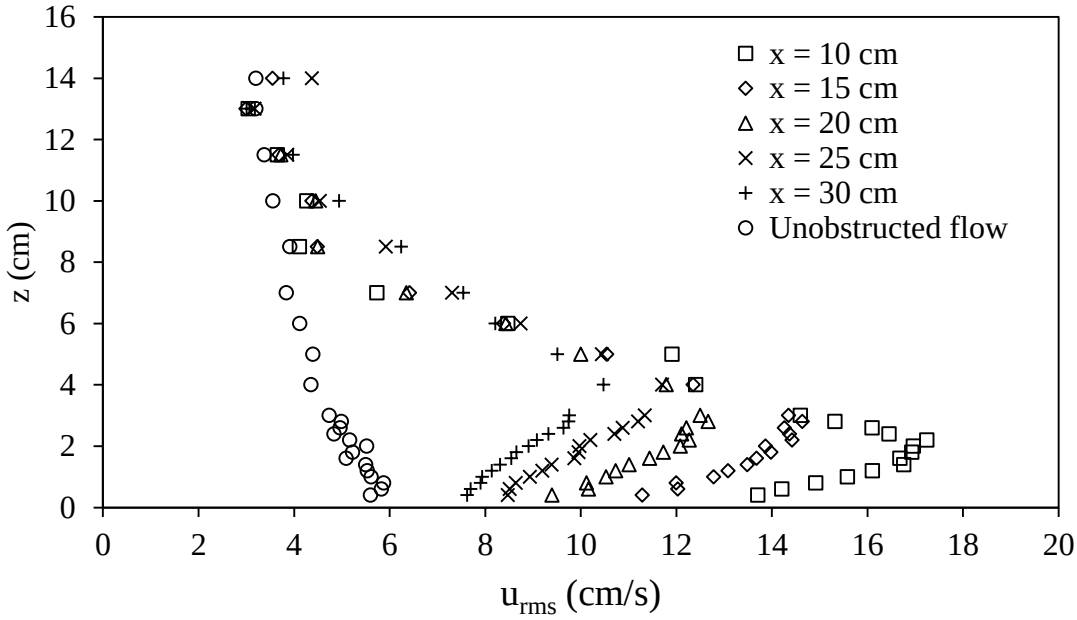

Fig. 3. Profiles of rms value of velocity fluctuation in the streamwise direction for U = 0.59 m/s and D = 0.23 mm

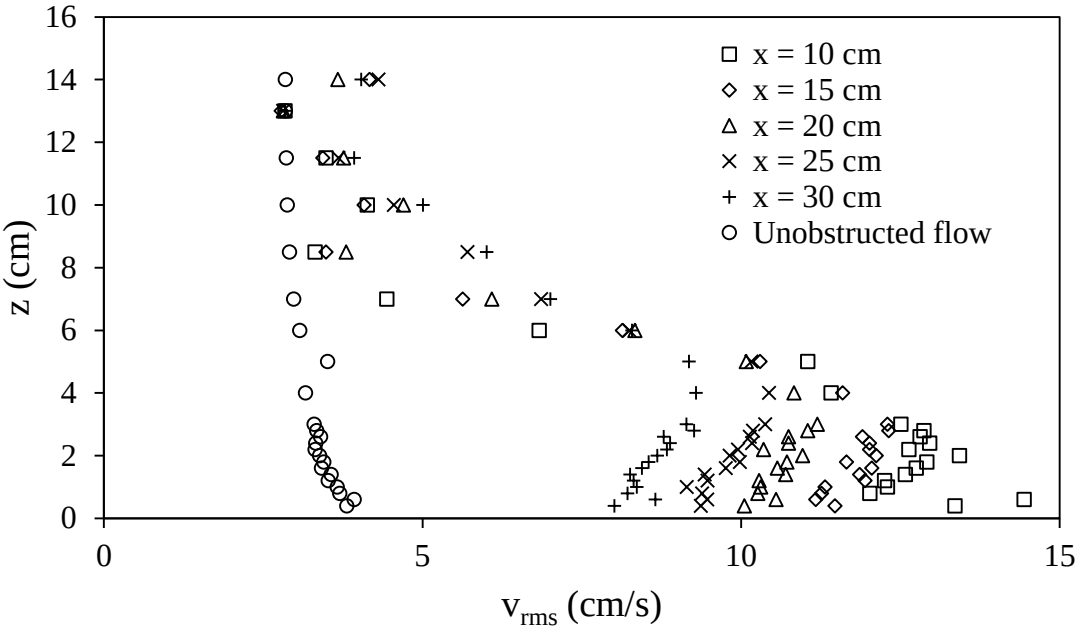

Fig. 4. Profiles of rms value of velocity fluctuation in the lateral direction for U = 0.59 m/s and D = 0.23 mm

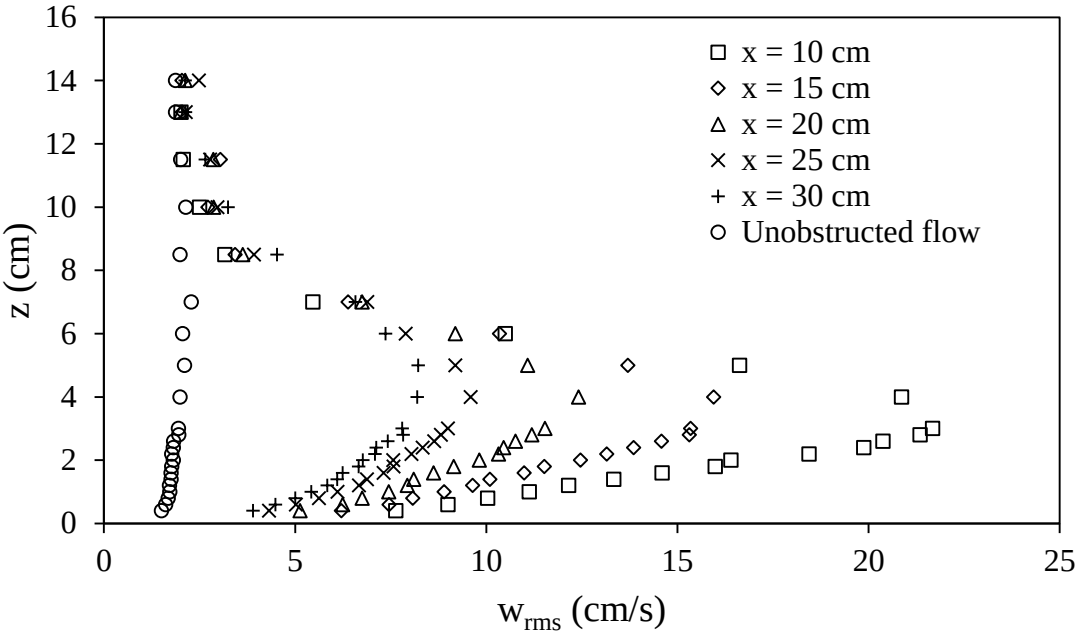

Fig. 5. Profiles of rms value of velocity fluctuation in the vertical direction for U = 0.59 m/s and D = 0.23 mm

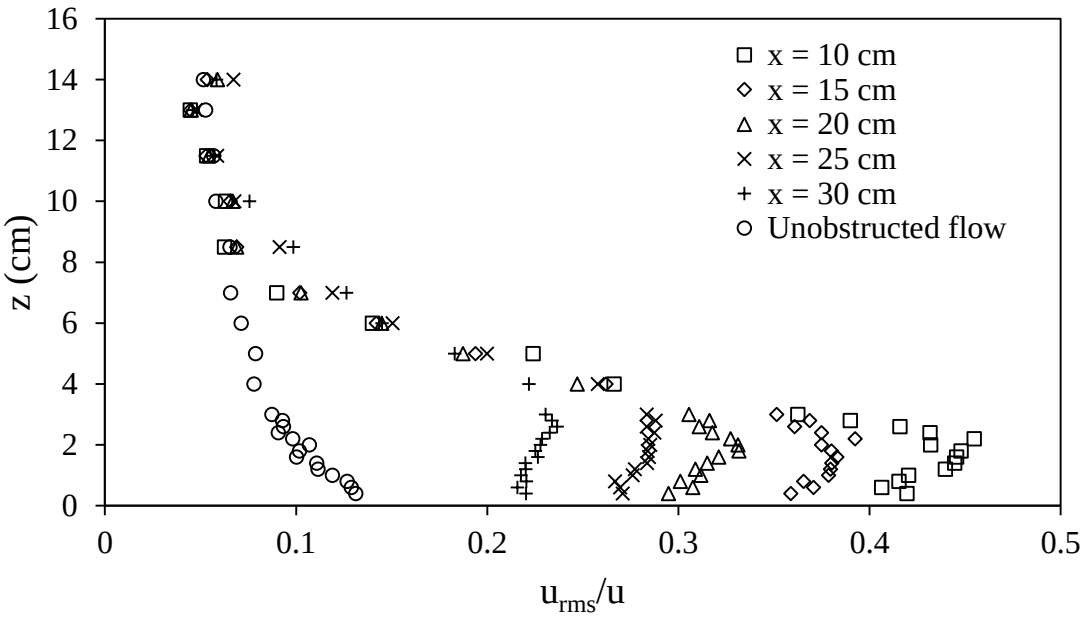

Fig. 6. Profiles of relative turbulence intensity in the streamwise direction for U = 0.59 m/s and D = 0.23 mm

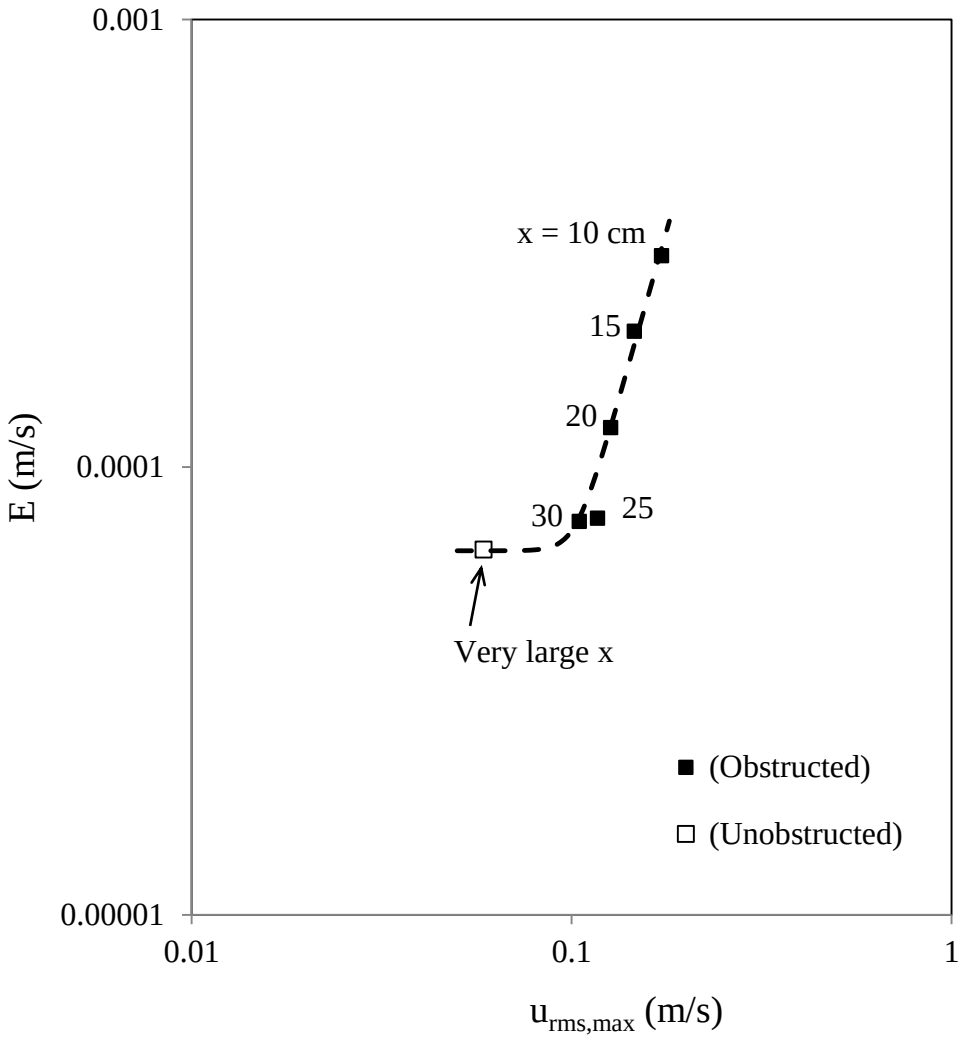

Fig. 7. Variation of E with the maximum value of u_{rms} for U = 0.59 m/s and D = 0.23 mm. The unobstructed flow represents a very large distance from the cylinder to the test section.

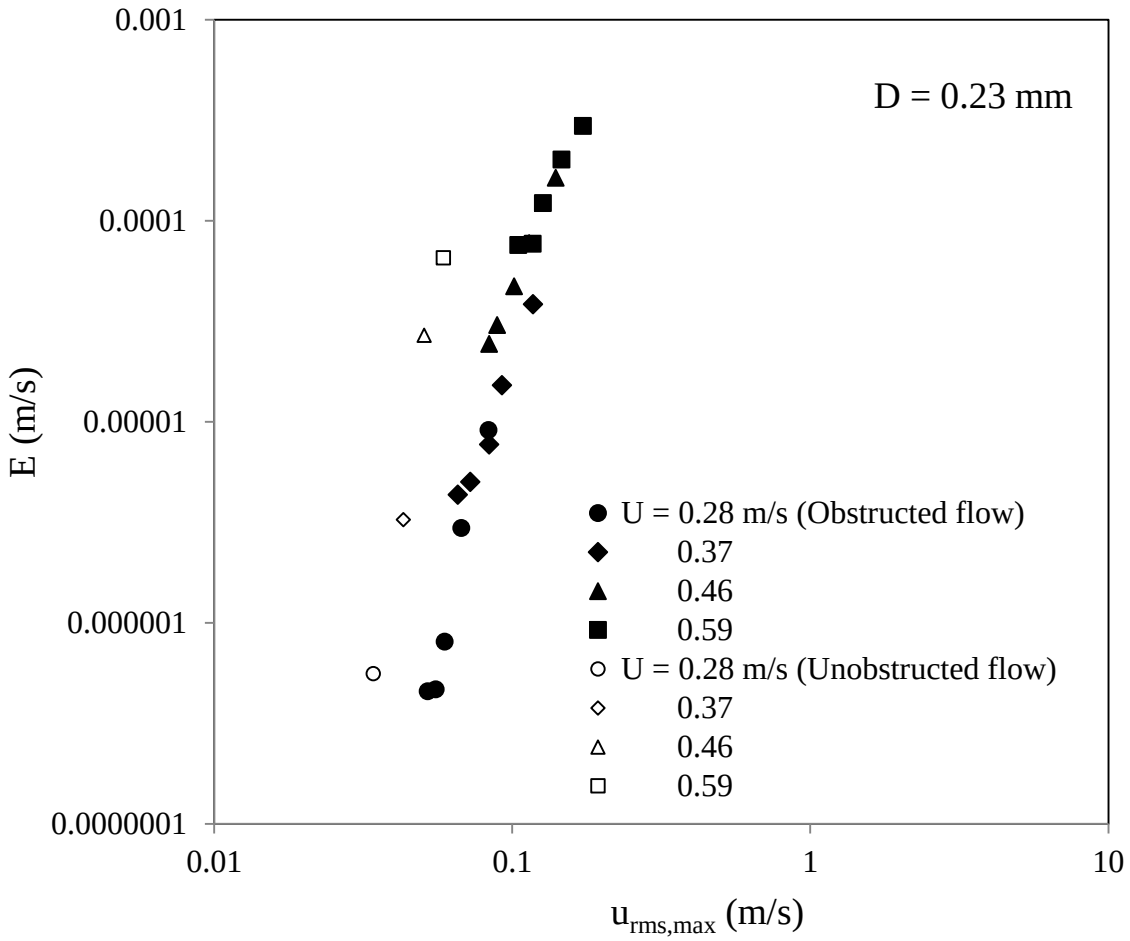

Fig. 8. Variation of E with $u_{rms,max}$ for D = 0.23 mm for obstructed and unobstructed flows with four flow rates.

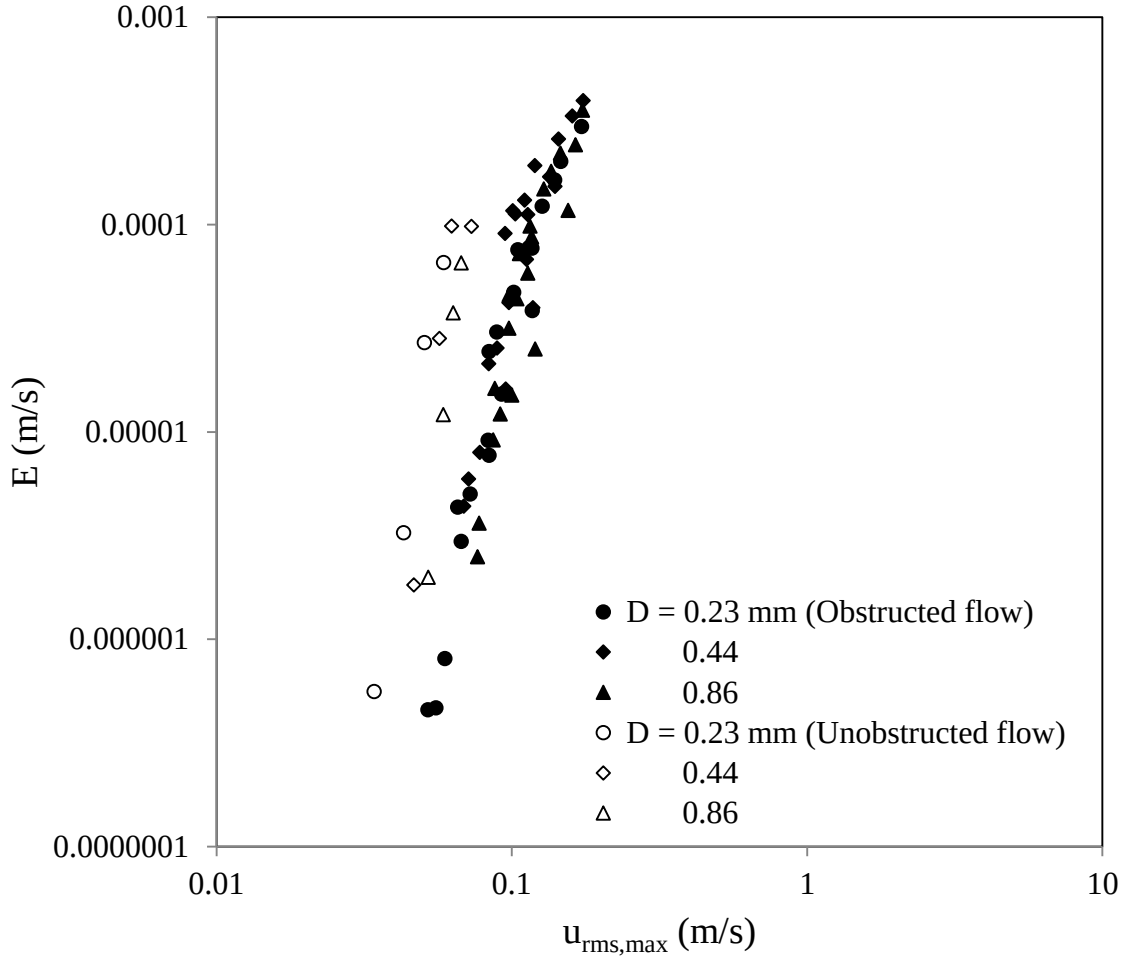

Fig. 9. Variation of E with $u_{rms,max}$ for three sediment sizes.

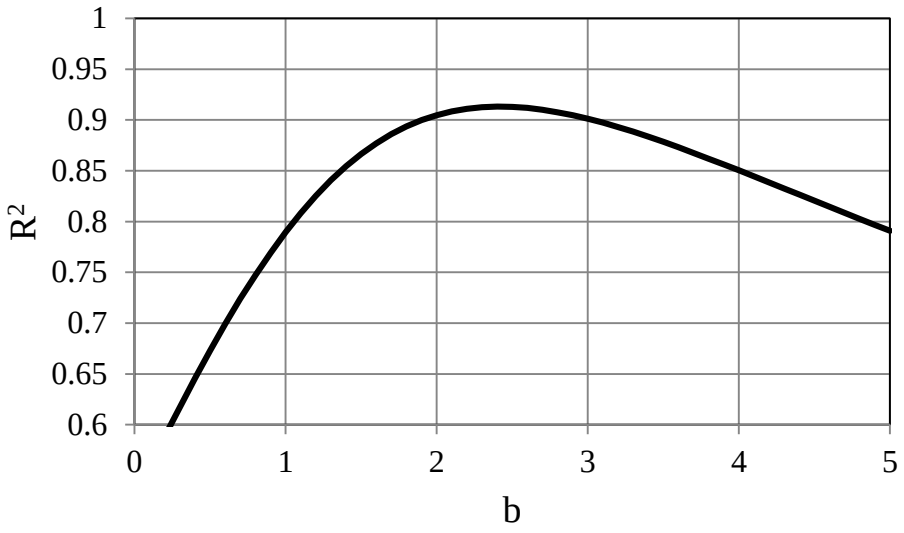

Fig. 10. R^2-value varying with the power b.

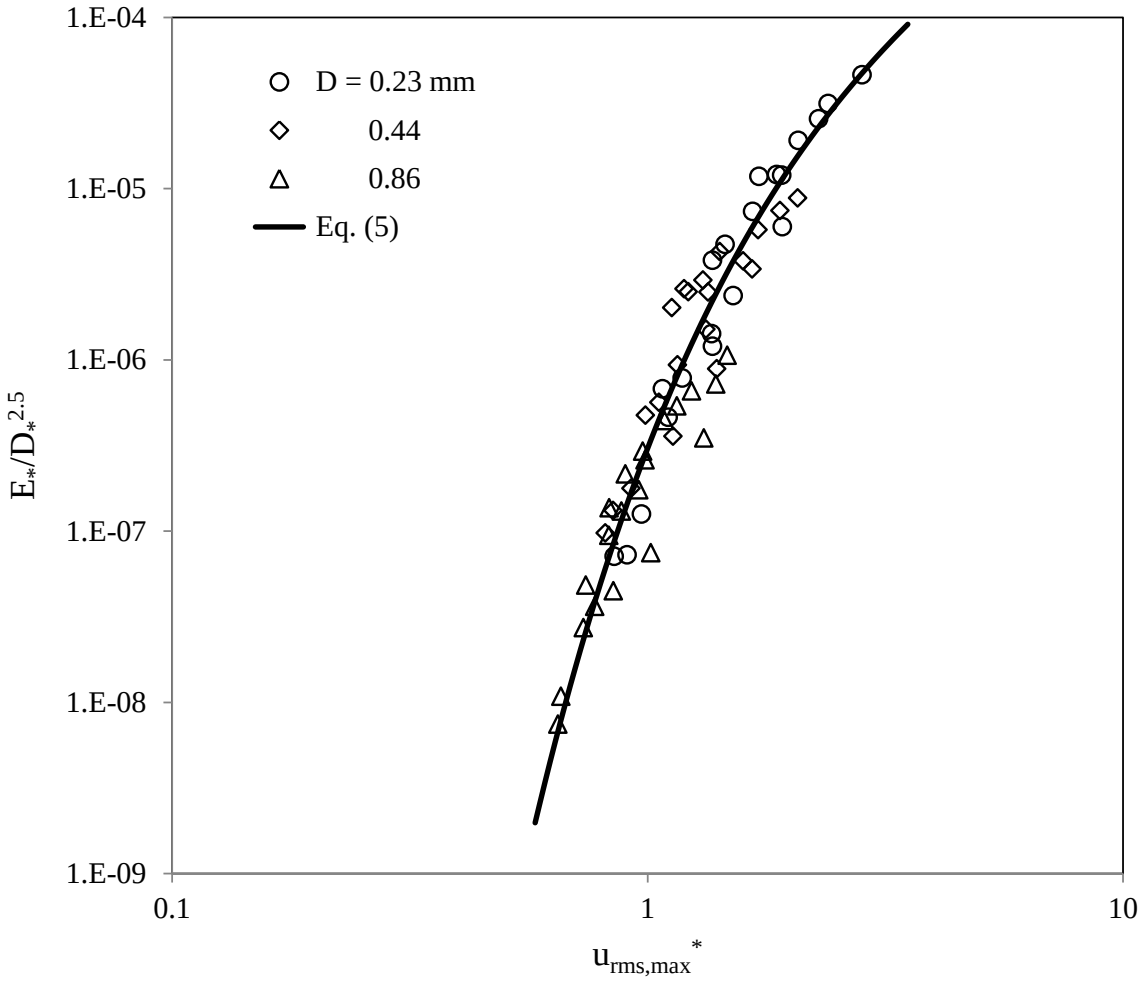

Fig. 11. Correlation based on maximum velocity fluctuation in the streamwise direction.

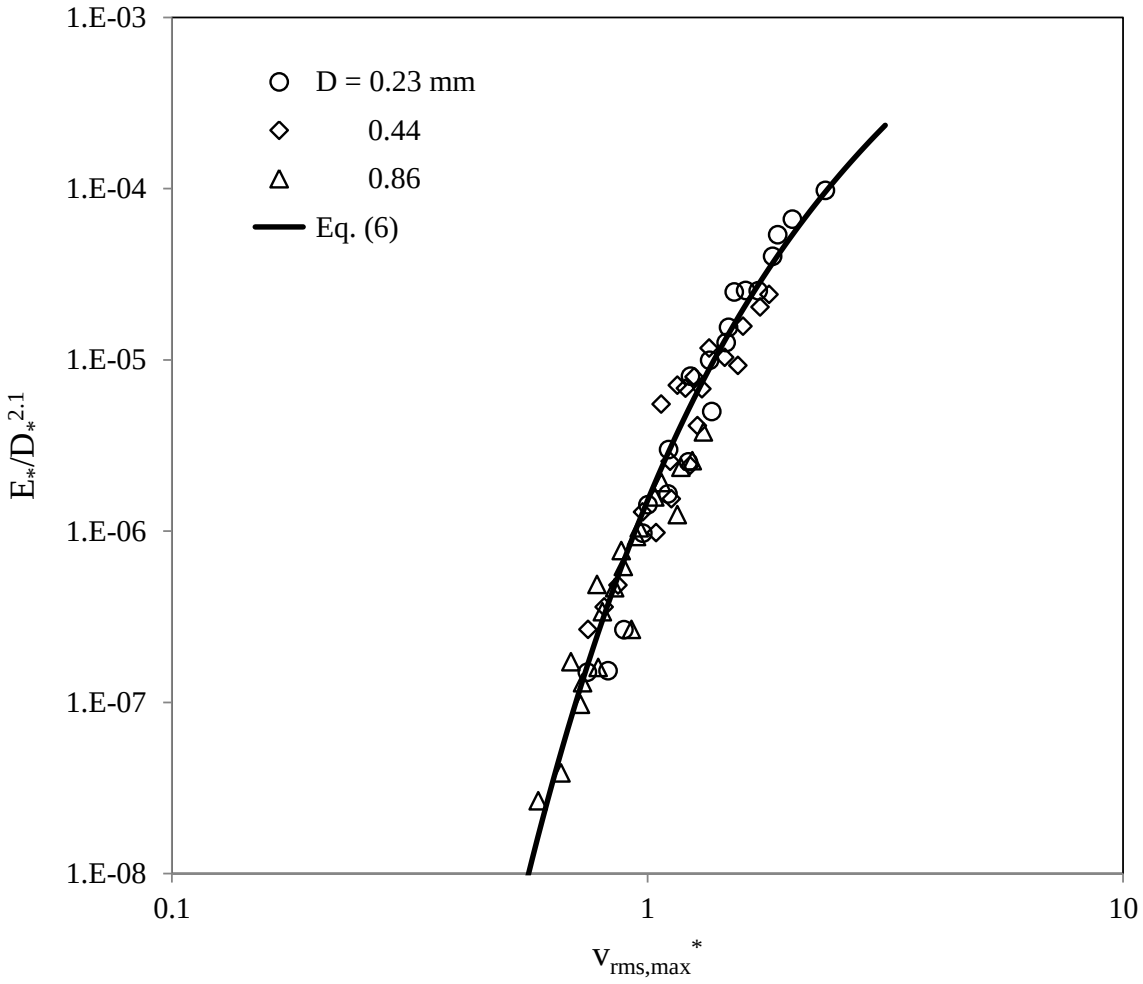

Fig. 12. Correlation based on maximum velocity fluctuation in the lateral direction.

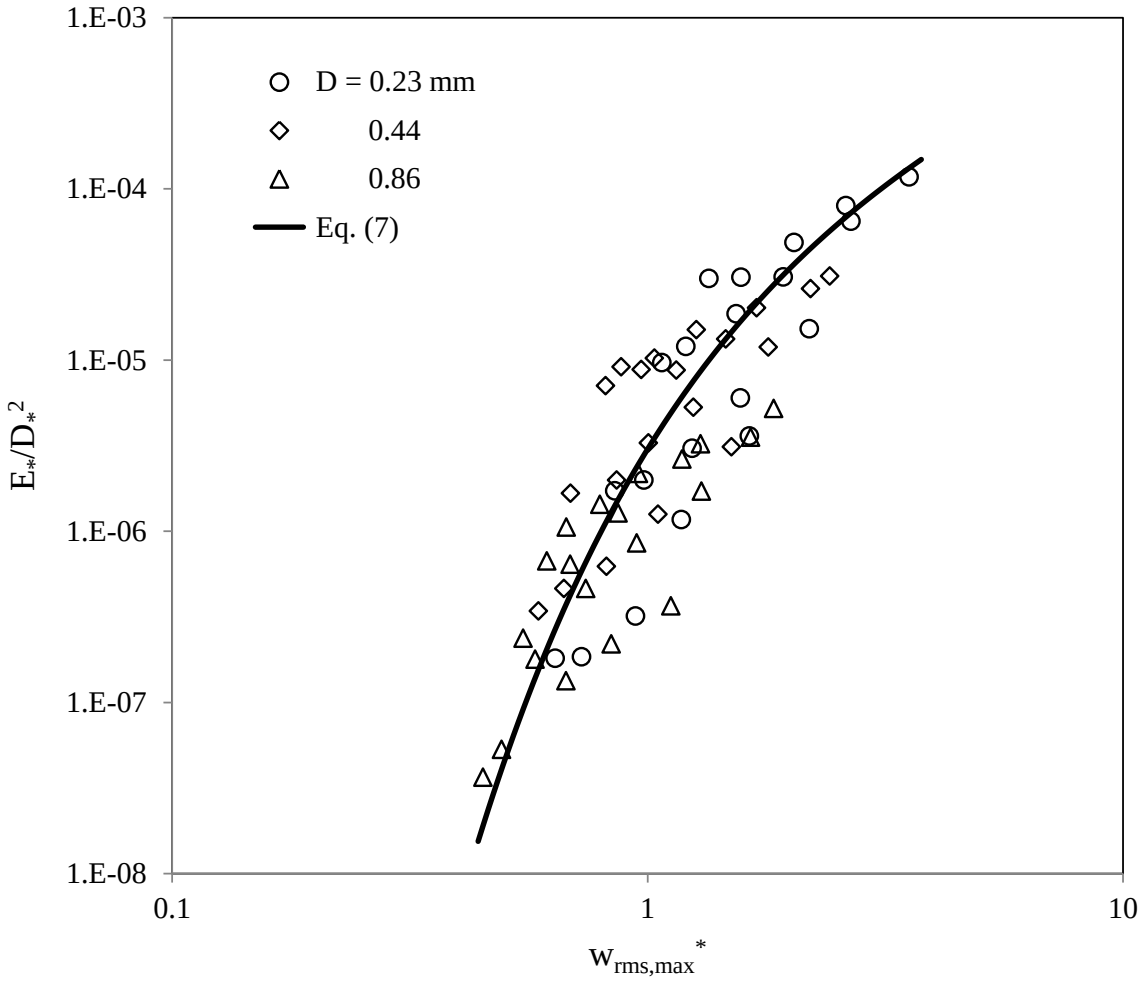

Fig. 13. Correlation based on maximum velocity fluctuation in the vertical direction

1

2 Table 1 Summary of experimental data

Series No.	Run No.	Flow rate Q (m^3/s)	Distance from cylinder to test section x (m)	Grain median diameter D (mm)	Shear velocity u_* (m/s)	Cross-sectional average velocity U (m/s)	Maximum of u_{rms} $u_{rms,max}$ (m/s)	Maximum of v_{rms} $v_{rms,max}$ (m/s)	Maximum of w_{rms} $w_{rms,max}$ (m/s)	Reynolds number UH/ν	Pickup rate E (m/s)
1	1	0.036	unobstructed	0.23	0.010	0.272	0.034	0.026	0.017	63,256	5.59E-07
	2	0.036	0.10	0.23		0.284	0.083	0.068	0.100	66,047	9.09E-06
	3	0.036	0.15	0.23		0.282	0.067	0.060	0.072	65,581	2.96E-06
	4	0.036	0.20	0.23		0.278	0.059	0.054	0.058	64,651	8.06E-07
	5	0.036	0.25	0.23		0.278	0.055	0.050	0.044	64,651	4.66E-07
	6	0.036	0.30	0.23		0.276	0.052	0.046	0.039	64,186	4.56E-07
2	7	0.047	unobstructed	0.23	0.014	0.365	0.043	0.030	0.013	84,884	3.26E-06
	8	0.047	0.10	0.23		0.371	0.117	0.089	0.134	86,279	3.84E-05
	9	0.047	0.15	0.23		0.372	0.092	0.083	0.096	86,512	1.52E-05
	10	0.047	0.20	0.23		0.370	0.084	0.074	0.076	86,047	7.70E-06
	11	0.047	0.25	0.23		0.370	0.072	0.067	0.060	86,047	5.02E-06
	12	0.047	0.30	0.23		0.368	0.066	0.061	0.052	85,581	4.34E-06
3	13	0.058	unobstructed	0.23	0.016	0.456	0.051	0.036	0.024	106,047	2.69E-05
	14	0.058	0.10	0.23		0.456	0.140	0.115	0.163	106,047	1.64E-04
	15	0.058	0.15	0.23		0.465	0.114	0.098	0.118	108,140	7.73E-05
	16	0.058	0.20	0.23		0.471	0.102	0.090	0.094	109,535	4.71E-05
	17	0.058	0.25	0.23		0.465	0.089	0.083	0.074	108,140	3.03E-05
	18	0.058	0.30	0.23		0.474	0.084	0.075	0.065	110,233	2.44E-05
4	19	0.067	unobstructed	0.23	0.023	0.586	0.059	0.039	0.023	136,279	6.55E-05
	20	0.067	0.10	0.23		0.608	0.172	0.144	0.217	141,395	2.97E-04
	21	0.067	0.15	0.23		0.599	0.146	0.123	0.159	139,302	2.01E-04

	22	0.067	0.20	0.23		0.592	0.127	0.112	0.124	137,674	1.23E-04
	23	0.067	0.25	0.23		0.587	0.117	0.104	0.096	136,512	7.69E-05
	24	0.067	0.30	0.23		0.589	0.105	0.093	0.082	136,977	7.56E-05
5	25	0.042	unobstructed	0.44	0.014	0.362	0.047	0.035	0.021	84,186	1.83E-06
	26	0.042	0.10	0.44		0.364	0.118	0.104	0.127	84,651	3.97E-05
	27	0.042	0.15	0.44		0.363	0.095	0.088	0.089	84,419	1.61E-05
	28	0.042	0.20	0.44		0.362	0.078	0.073	0.069	84,186	7.96E-06
	29	0.042	0.25	0.44		0.361	0.071	0.068	0.056	83,953	5.92E-06
	30	0.042	0.30	0.44		0.364	0.069	0.063	0.050	84,651	4.38E-06
6	31	0.053	unobstructed	0.44	0.019	0.458	0.057	0.043	0.025	106,512	2.82E-05
	32	0.053	0.10	0.44		0.470	0.140	0.131	0.151	109,302	1.53E-04
	33	0.053	0.15	0.44		0.466	0.112	0.108	0.105	108,372	6.78E-05
	34	0.053	0.20	0.44		0.465	0.098	0.094	0.085	108,140	4.20E-05
	35	0.053	0.25	0.44		0.463	0.089	0.095	0.073	107,674	2.54E-05
	36	0.053	0.30	0.44		0.462	0.084	0.082	0.058	107,442	2.13E-05
7	37	0.064	unobstructed	0.44	0.022	0.532	0.063	0.048	0.025	124,340	9.82E-05
	38	0.064	0.10	0.44		0.556	0.160	0.146	0.186	129,949	3.34E-04
	39	0.064	0.15	0.44		0.555	0.134	0.123	0.123	129,715	1.70E-04
	40	0.064	0.20	0.44		0.548	0.113	0.110	0.097	128,079	1.12E-04
	41	0.064	0.25	0.44		0.551	0.103	0.102	0.082	128,780	1.12E-04
	42	0.064	0.30	0.44		0.543	0.095	0.090	0.069	126,910	9.06E-05
8	43	0.068	unobstructed	0.44	0.025	0.583	0.073	0.061	0.026	135,581	9.79E-05
	44	0.068	0.10	0.44		0.597	0.175	0.152	0.204	138,837	3.96E-04
	45	0.068	0.15	0.44		0.598	0.144	0.134	0.143	139,070	2.58E-04
	46	0.068	0.20	0.44		0.592	0.120	0.114	0.107	137,674	1.93E-04
	47	0.068	0.25	0.44		0.586	0.110	0.106	0.087	136,279	1.31E-04
	48	0.068	0.30	0.44		0.584	0.101	0.098	0.074	135,814	1.17E-04
9	49	0.047	unobstructed	0.86	0.019	0.400	0.052	0.039	0.022	93,023	1.99E-06
	50	0.047	0.10	0.86		0.407	0.120	0.109	0.132	94,651	2.51E-05
	51	0.047	0.15	0.86		0.410	0.100	0.093	0.099	95,349	1.50E-05

	52	0.047	0.20	0.86		0.406	0.086	0.085	0.080	94,419	9.13E-06
	53	0.047	0.25	0.86		0.404	0.078	0.078	0.058	93,953	3.63E-06
	54	0.047	0.30	0.86		0.402	0.076	0.070	0.053	93,451	2.50E-06
10	55	0.054	unobstructed	0.86	0.022	0.467	0.059	0.044	0.027	108,667	1.21E-05
	56	0.054	0.10	0.86		0.486	0.155	0.136	0.153	113,014	1.17E-04
	57	0.054	0.15	0.86		0.480	0.113	0.105	0.112	111,523	5.83E-05
	58	0.054	0.20	0.86		0.475	0.098	0.095	0.088	110,465	3.17E-05
	59	0.054	0.25	0.86		0.480	0.091	0.086	0.068	111,512	1.22E-05
	60	0.054	0.30	0.86		0.473	0.088	0.082	0.065	109,977	1.62E-05
11	61	0.065	unobstructed	0.86	0.024	0.549	0.063	0.047	0.025	127,651	3.74E-05
	62	0.065	0.10	0.86		0.576	0.164	0.147	0.194	133,930	2.42E-04
	63	0.065	0.15	0.86		0.577	0.136	0.126	0.139	134,163	1.80E-04
	64	0.065	0.20	0.86		0.572	0.117	0.112	0.102	133,116	8.72E-05
	65	0.065	0.25	0.86		0.585	0.104	0.101	0.081	136,070	4.38E-05
	66	0.065	0.30	0.86		0.553	0.098	0.092	0.072	128,698	4.58E-05
12	67	0.071	unobstructed	0.86	0.030	0.593	0.067	0.052	0.029	137,791	6.52E-05
	68	0.071	0.10	0.86		0.634	0.174	0.155	0.217	147,442	3.56E-04
	69	0.071	0.15	0.86		0.638	0.146	0.139	0.153	148,256	2.21E-04
	70	0.071	0.20	0.86		0.615	0.128	0.122	0.113	143,093	1.48E-04
	71	0.071	0.25	0.86		0.611	0.115	0.113	0.094	142,093	9.81E-05
	72	0.071	0.30	0.86		0.588	0.106	0.104	0.080	136,698	7.23E-05

3

4